

# Image Coding for Machines via Feature-Preserving Rate-Distortion Optimization

Samuel Fernández-Mendiña, *Student Member, IEEE*, Eduardo Pavez, *Member, IEEE*,  
and Antonio Ortega, *Fellow, IEEE*

**Abstract**—Many images and videos are primarily processed by computer vision algorithms, involving only occasional human inspection. When this content requires compression before processing, e.g., in distributed applications, coding methods must optimize for both visual quality and downstream task performance. We first show that, given the features obtained from the original and the decoded images, an approach to reduce the effect of compression on a task loss is to perform rate-distortion optimization (RDO) using the distance between features as a distortion metric. However, optimizing directly such a rate-distortion trade-off requires an iterative workflow of encoding, decoding, and feature evaluation for each coding parameter, which is computationally impractical. We address this problem by simplifying the RDO formulation to make the distortion term computable using block-based encoders. We first apply Taylor’s expansion to the feature extractor, recasting the feature distance as a quadratic metric with the Jacobian matrix of the neural network. Then, we replace the linearized metric with a block-wise approximation, which we call input-dependent squared error (IDSE). To reduce computational complexity, we approximate IDSE using Jacobian sketches. The resulting loss can be evaluated block-wise in the transform domain and combined with the sum of squared errors (SSE) to address both visual quality and computer vision performance. Simulations with AVC across multiple feature extractors and downstream neural networks show up to 10% bit-rate savings for the same computer vision accuracy compared to RDO based on SSE, with no decoder complexity overhead and just a 7% encoder complexity increase.

**Index Terms**—RDO, coding for machines, feature distance, Jacobian, rate-distortion, image compression, sketching

## I. INTRODUCTION

Many images and videos are now primarily consumed by machine learning systems to perform pattern recognition tasks. When such content requires compression before algorithmic processing, coding methods may compromise visual quality for computer vision (CV) performance, a framework known as *coding for machines* (CM) [1]–[3]. While similar ideas were explored for classical learning methods [4], advances in deep neural networks (DNNs) [5] applied to CV have sparked renewed interest [6]–[8]. Different coding strategies are possible depending on whether the image has to be transmitted and how much the encoder knows about the target task or tasks. When transmitting the image is not required,

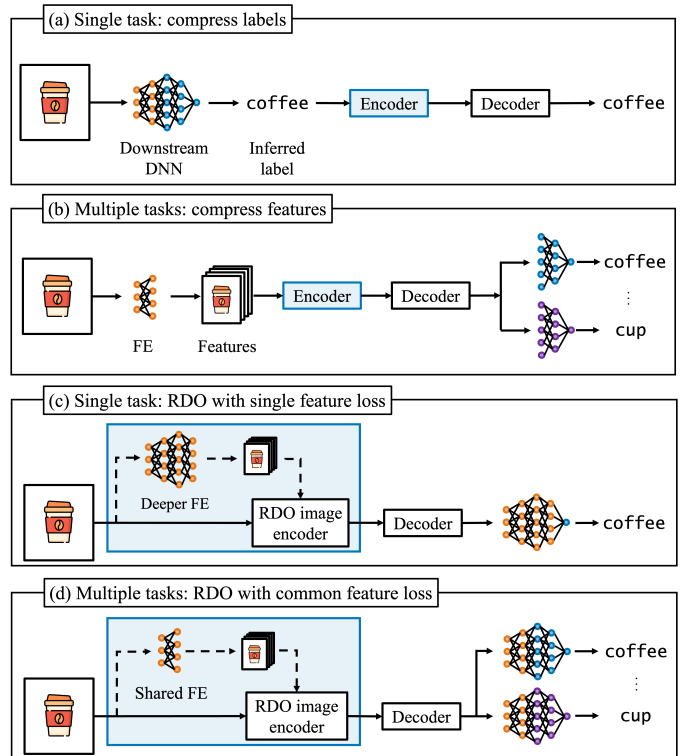


Fig. 1: Examples of CM methods when image transmission is (a-b) not needed and (c-d) needed. FE = feature extractor.

algorithms based on the information bottleneck method [9] are sufficient. For instance, for single-task classification problems, encoding the inferred labels is optimal [10] (Fig. 1a). For families of related CV tasks, it can be more efficient to compress *feature vectors*, e.g., the outputs of the earlier layers of a DNN [11] (Fig. 1b). Similarly, when the target tasks are unknown, features trained for invariance—e.g., using self-supervised learning (SSL) [12]—can be extracted, compressed, and transmitted [10], [13].

We consider instead applications that require image transmission [1], enabling additional human supervision for the task (cf. Fig. 1c–d). We focus on distributed communication settings with power and bandwidth constraints. Since images have to be transmitted anyway, it is often preferable to perform the CV task remotely on the decompressed image [7] (Fig. 1c), which is also more efficient given the complexity of running a full-fledged DNN at the sensing system [2]. This approach is particularly advantageous when running several CV tasks

This work was funded in part by the Fulbright Commission in Spain.

S. Fernández-Mendiña, E. Pavez, and A. Ortega are with the Ming Hsieh Department of Electrical and Computer Engineering, University of Southern California, Los Angeles, 90089, United States (email: samuelf9@usc.edu; pavezcar@usc.edu; aortega@usc.edu).

Manuscript received Month XX, 20XX; revised Month XX, 20XX.

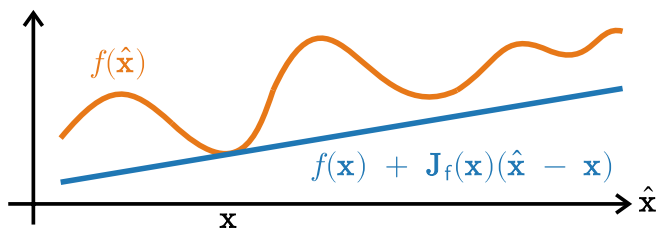


Fig. 2: Linear approximation of the features of the compressed image via Taylor's expansion around the input image.

on the same image, as it avoids executing multiple DNNs on the edge device (Fig. 1d). Examples of this setup are object detection/instance segmentation in video surveillance, traffic monitoring, or autonomous navigation [14].

For our scenarios of interest (Fig. 1c-d), the encoder should be optimized to preserve information relevant to *both* the CV task and visual quality [4]. Thus, distortion metrics conventionally used for rate-distortion optimization (RDO) [15], [16], such as the sum of squared errors (SSE), must be complemented or replaced by task-specific losses. Based on heuristic arguments, prior work proposed the distance between features obtained from the original and the decoded images (feature distance, FD) [17], [18] as an alternative distortion metric that can be incorporated into RDO to account for CV performance. Since features are extracted from full images but modern codecs can control bit allocation at the block level, [17] proposes to compute FD using the features extracted from the decoded image for each block-wise coding configuration. While allowing RDO with a distortion metric relevant to CV, this setup requires an iterative workflow of encoding, decoding, and feature extraction for each coding option, which is computationally impractical. [17] addresses this problem by computing block-wise shallow features, which limits performance since the target tasks are completed with deep features extracted from the whole image (cf. Sec. I-A3).

In this paper, we show theoretically that minimizing FD can preserve task performance. This analysis can also guide feature selection; for instance, when multiple tasks can be addressed with DNNs sharing common earlier layers, as in transfer learning [19], using these common layers as a feature extractor can preserve performance in all transferred tasks (Fig. 1d). To make FD practical for block-level RDO, we first apply Taylor's expansion to recast FD as a quadratic loss involving the Jacobian matrix of the feature extractor with respect to the input image (Fig. 2). Then, we replace this linearized metric with a block-wise approximation, which we call *input-dependent squared error* (IDSE). We use sketching techniques [20] to avoid computing the entire Jacobian matrix. The resulting metric can be seen as an importance map, where pixels are weighted differently based on their relevance for the target tasks. IDSE can be evaluated block-wise in the transform domain; by combining it with an SSE term, the codec can optimize for both perceptual quality and CV tasks while remaining compatible with standard-compliant decoders.

Results using an AVC codec show that using RDO with IDSE to choose block-level partitioning and quantization step-

size provides up to 10% bit-rate savings with respect to RDO with SSE while preserving the same accuracy for object detection/instance segmentation tasks in the COCO 2017 validation set [21] and the PennFudan dataset [22]. Although we focus on AVC, feature-preserving RDO can be used in systems with more coding options, such as VVC [23] (cf. Sec. VI).

This paper extends our prior work [18] with: 1) *theoretical foundations*, including justifications for minimizing FD as a proxy to preserve task loss (Sec. III-A) and for block-wise localization (Sec. III-C), 2) *input-adaptive methods*, including the selection of the regularization parameter controlling the IDSE-SSE trade-off (Sec. IV-A) and the Lagrangian (Sec. IV-C), and 3) *extended experiments*, including feature extractors of various depths (Sec. V-B) and architectural complexities (Sec. V-A2), an analysis of the trade-off between visual quality and downstream DNN performance (Sec. V-A3), and tests with a task mismatch between the network used for feature preservation and the downstream DNN (Sec. V-B2).

#### A. Related work

1) *Neural compression*: Both generative [24] and input-dependent [25] neural compression methods [24] can be trained end-to-end to optimize a downstream task [3], [26]. However, computational cost limits their deployment in power-constrained platforms [27]: generative methods require millions of multiply and add operations per pixel on both the encoder and the decoder, while input-dependent encoders [25] remain too complex for the lower-end devices used in distributed applications. Moreover, each encoder/decoder pair is optimized for particular tasks [1], [28] and may underperform on tasks outside its training scope.

2) *Modified traditional codecs*: Several methods have been proposed to modify conventional codecs, which are less computationally demanding than learned approaches. Ahonen et al. [29] enhance decompressed images using learned filters, which results in better performance on the task but cannot be used to optimize bit allocation. Other approaches allow the encoder to be modified. For example, [30] modifies JPEG quantization tables using a proxy codec, which cannot be easily extended to modern video compression systems with intra/inter-prediction. Alternatively, [7] chooses quantization steps at the block level but does not allow optimizing other codec parameters such as block partitioning or prediction mode. All these approaches fall short in optimizing compression efficiency relative to RDO-based methods such as [17].

3) *RDO based on FD*: Closest to our approach, [17] achieves block-level RDO by evaluating the feature extractor block-wise (block FD). Nonetheless, extracting features independently for each block overlooks relationships between blocks and requires using relatively shallow features. As a result, [17] cannot directly evaluate the final importance of each block for a target task, which is determined in deeper layers. Moreover, DNN non-linearities often lead to concave or non-monotonic rate-distortion (RD) landscapes, so increasing rates may no longer reduce FD. Thus, the RD trade-off becomes harder to navigate. For instance, only a subset of low/high rate operating points may be reachable (Fig. 3),

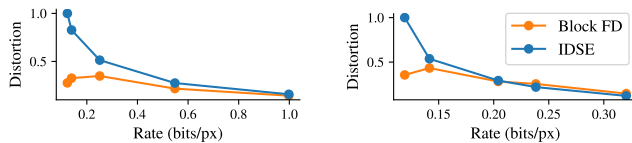


Fig. 3: RD curves using SSE-RDO AVC for block FD and IDSE with a feature pyramid network (FPN) [31] as feature extractor, for blocks of  $32 \times 32$  pixels. Neural network nonlinearities can make block FD concave or non-monotonic with the rate, reducing the number of possible operating points. IDSE is quadratic by design and has monotonic behavior.

Distortion	Block RDO	Trans. RDO	Quad.	Global	Target
FD	✗	✗	✗	✓	Machines
Block FD [17]	✓	✗	✗	✗	Machines
SSE	✓	✓	✓	✓	Humans
IDSE (ours)	✓	✓	✓	✓	Machines

Table I: RDO methods in CM. Some approaches use quadratic metrics (**Quad.**), can be applied in the transform domain (**Trans.**), and are based on features extracted from the whole image (**Global**). Like SSE, IDSE is convenient for RDO, and it can account for CV task performance.

leading to reconstructions with a large SSE even for high rates, which impacts visual quality. Block FD may also become computationally intensive [32] since it requires pixel-domain evaluation of the DNN for each RDO candidate.

In contrast to [17], which computes the FD explicitly for each block *using the output of shallow layers* as approximately-local features, our IDSE-based approach uses *backpropagation* via autodiff [33] to determine the importance of each pixel (per-pixel importance map) given *any feature extractor* (shallow, intermediate, or deep). As opposed to FD and block FD, IDSE is guaranteed to be quadratic with the pixel-wise error, making the RD curves convex and monotonic. Similar to SSE, RDO with IDSE can run block-wise in the transform domain. Furthermore, by relying on the features obtained from the whole image, it can account for the final importance of each block for the target computer vision tasks, which [17] cannot do (cf. Table I for a comparison).

## B. Organization and notation

**Organization.** Sec. II explains RDO and Sec. III feature-preserving RDO. Sec. IV reviews IDSE in a coding pipeline. Sec. V includes experiments and Sec. VI conclusions.

**Notation** (cf. Table II). Uppercase bold letters, such as  $\mathbf{A}$ , denote matrices. Lowercase bold letters, such as  $\mathbf{a}$ , denote vectors. The  $n$ th entry of  $\mathbf{a}$  is  $a_n$ , and the  $(i, j)$ th entry of  $\mathbf{A}$  is  $A_{ij}$ . Regular letters denote scalar values.

## II. RATE-DISTORTION OPTIMIZATION

Let  $\mathbf{x}$  be an image with  $n_p$  pixels and  $\hat{\mathbf{x}}(\boldsymbol{\theta})$  its compressed version using parameters  $\boldsymbol{\theta} \in \Theta$ , where  $\Theta \subset \mathbb{N}^{n_b}$  is the set of all possible operating points and  $n_b$  is the number of blocks.

Symbol	Description
$n_b$	Number of blocks in the input
$n_f$	Dimensionality of feature space
$n_p$	Number of pixels in the input
$n_{pb}$	Number of pixels in a block
$n_r$	Number of RDO candidates per block
$n_s$	Feature dimensionality after sketching
$n_t$	Number of downstream tasks
$\mathbf{x} \in \mathbb{R}^{n_p}$	Codec input
$\mathbf{x}_i \in \mathbb{R}^{n_{pb}}$	$i$ th block of the input
$\hat{\mathbf{x}}(\boldsymbol{\theta}) \in \mathbb{R}^{n_p}$	Compressed version of $\mathbf{x}$ with parameters $\boldsymbol{\theta}$
$\hat{\mathbf{x}}_i(\theta_i) \in \mathbb{R}^{n_{pb}}$	$i$ th block of the compressed image
$f(\mathbf{x}) \in \mathbb{R}^{n_f}$	Features extracted from $\mathbf{x}$
$\mathbf{J}_f(\mathbf{x}) \in \mathbb{R}^{n_f \times n_p}$	Jacobian of $f(\cdot)$ evaluated at $\mathbf{x}$
$\mathbf{J}_f^{(i)}(\mathbf{x}) \in \mathbb{R}^{n_f \times n_{pb}}$	Columns of $\mathbf{J}_f(\mathbf{x})$ for the $i$ th block of the input
$\mathbf{J}_s(\mathbf{x}) \in \mathbb{R}^{n_s \times n_p}$	Sketched version of $\mathbf{J}_f(\mathbf{x})$
$\mathbf{J}_s^{(i)}(\mathbf{x}) \in \mathbb{R}^{n_s \times n_{pb}}$	Columns of $\mathbf{J}_s(\mathbf{x})$ for the $i$ th block of the input

Table II: List of symbols and their meaning.

Assume every entry of  $\boldsymbol{\theta}$  takes values in the set  $\{1, \dots, n_r\}$ , where  $n_r$  denotes the number of RDO options. Given blocks of size  $n_{pb}$ ,  $\mathbf{x}_i \in \mathbb{R}^{n_{pb}}$  for  $i = 1, \dots, n_b$ , we aim to find parameters  $\boldsymbol{\theta}^*$  satisfying [15]:

$$\boldsymbol{\theta}^* = \arg \min_{\boldsymbol{\theta} \in \Theta} d(\hat{\mathbf{x}}(\boldsymbol{\theta}), \mathbf{x}) + \lambda \sum_{i=1}^{n_b} r_i(\hat{\mathbf{x}}_i(\boldsymbol{\theta})), \quad (1)$$

where  $d(\cdot, \cdot)$  is the distortion metric,  $r_i(\cdot)$  is the rate for the  $i$ th coding unit, and  $\lambda \geq 0$  is the Lagrange multiplier controlling the RD trade-off. We are especially interested in distortion metrics that decompose as the sum of block-wise distortions,

$$d(\hat{\mathbf{x}}_1(\boldsymbol{\theta}), \dots, \hat{\mathbf{x}}_{n_b}(\boldsymbol{\theta}), \mathbf{x}_1, \dots, \mathbf{x}_{n_b}) = \sum_{i=1}^{n_b} d_i(\hat{\mathbf{x}}_i(\boldsymbol{\theta}), \mathbf{x}_i), \quad (2)$$

which is true for SSE but may not hold for other metrics. When each coding unit can be optimized independently, we obtain  $\hat{\mathbf{x}}_i(\boldsymbol{\theta}) = \hat{\mathbf{x}}_i(\theta_i)$  [15], [16], which leads to

$$\theta_i^* = \arg \min_{\theta_i \in \Theta_i} d_i(\hat{\mathbf{x}}_i(\theta_i), \mathbf{x}_i) + \lambda r_i(\hat{\mathbf{x}}_i(\theta_i)), \quad (3)$$

for  $i = 1, \dots, n_b$ , where  $\Theta_i$  is the set of all parameters for the  $i$ th block. This is the RDO formulation most video codecs solve [15]. A practical way to choose  $\lambda$  is [16]:

$$\lambda = c 2^{(QP-12)/3}, \quad (4)$$

where QP is the quality parameter, and  $c$  varies with the type of frame and content [34]. This work aims to replicate this block-level RDO formulation in a CM scenario using distortion metrics derived from computer vision tasks.

## III. FEATURE-PRESERVING RDO

We formulate our CM problem in Sec. III-A. Then, we introduce linearization (Sec. III-B), block-wise approximation (Sec. III-C), and Jacobian sketching (Sec. III-D).

### A. Problem formulation

Let the *feature extractor* be a function  $f(\cdot)$  mapping images with  $n_p$  pixels to  $n_f$ -dimensional representations. In this work, we focus on feature extractors comprising a set of the earlier layers of a DNN-based system. Assume we target  $n_t$  tasks, each of them with task loss  $\ell_k(\cdot, \cdot)$ , e.g., cross-entropy loss (CEL) or SSE, for  $k = 1, \dots, n_t$ . Given an input  $\mathbf{x}$  with ground truth labels  $\mathbf{y}_k$  and DNNs  $g_k(\cdot)$ , the loss is given by  $\ell_k(\mathbf{y}_k, g_k(\mathbf{x}))$ , for all  $k$ . Let the feature extractor be shared, such that the DNNs can be written as  $g_k(\mathbf{x}) = h_k(f(\mathbf{x}))$  for all  $k$ . We evaluate the degradation in performance due to compression via the consistency loss  $r_k(\hat{\mathbf{x}}, \mathbf{x}) \doteq \|\ell_k(\mathbf{y}_k, g_k(\hat{\mathbf{x}})) - \ell_k(\mathbf{y}_k, g_k(\mathbf{x}))\|_2^2$ , for all  $k$ , which is the metric of choice when approximating the output of one system using another—e.g., network distillation [35]. Next, we relate consistency loss to feature distance (FD).

**Proposition III.1.** *Let  $\ell_k(\cdot, \cdot)$  and  $h_k(\cdot)$  be Lipschitz continuous functions with constants  $L_k$  and  $H_k$ , respectively, for  $k = 1, \dots, n_t$ . Then,*

$$r_k(\hat{\mathbf{x}}, \mathbf{x}) \leq H_k^2 L_k^2 \|f(\hat{\mathbf{x}}) - f(\mathbf{x})\|_2^2, \quad \text{for } k = 1, \dots, n_t. \quad (5)$$

*Proof.* The result follows by consecutively applying Lipschitz continuity for  $\ell_k(\mathbf{y}_k, \cdot)$  and  $h_k(\cdot)$  for all  $k$ .  $\square$

The task losses (SSE and CEL) [36] and neural networks [37] we consider in this work are Lipschitz continuous. From Proposition III.1, we conclude that *minimizing feature distance can preserve task performance*. Hence, we write the CM problem as minimizing the FD subject to a rate constraint:

$$\theta^* = \arg \min_{\theta \in \Theta} \|f(\hat{\mathbf{x}}(\theta)) - f(\mathbf{x})\|_2^2 + \lambda \sum_{i=1}^{n_b} r_i(\hat{\mathbf{x}}_i(\theta_i)). \quad (6)$$

This approach allows choosing a feature extractor based on prior task knowledge. For instance, when pre-trained early layers are used across a series of tasks—e.g., transfer learning [19]—we use an IDSE based on the pixel importance for these early layers to preserve performance across all tasks.

The feature distance in (6) does not satisfy the locality property in (2): to evaluate it, we need the complete decoded image in the pixel domain. As a result, RDO with FD requires an iterative workflow of encoding, decoding, and feature distance evaluation, which is computationally impractical. In the following, we propose an alternative solution.

### B. Linearizing the feature extractor

We assume the feature extractor has second-order partial derivatives almost everywhere, which is satisfied by the DNNs we consider in this work [38]. Define the Jacobian matrix of  $f(\cdot)$  evaluated at the input image  $\mathbf{x}$  as  $\mathbf{J}_f(\mathbf{x}) \in \mathbb{R}^{n_f \times n_p}$ , where:

$$J_{ij}(\mathbf{x}) = \frac{\partial f_i(\mathbf{x})}{\partial x_j}, \quad i = 1, \dots, n_f, \quad j = 1, \dots, n_p. \quad (7)$$

Rewriting  $\hat{\mathbf{x}}(\theta) = \mathbf{x} + (\hat{\mathbf{x}}(\theta) - \mathbf{x})$ , we can apply Taylor's expansion to the feature extractor around  $\mathbf{x}$  (Fig. 2):

$$f(\hat{\mathbf{x}}(\theta)) = f(\mathbf{x}) + \mathbf{J}_f(\mathbf{x})(\hat{\mathbf{x}}(\theta) - \mathbf{x}) + o(\|\hat{\mathbf{x}}(\theta) - \mathbf{x}\|_2^2), \quad (8)$$

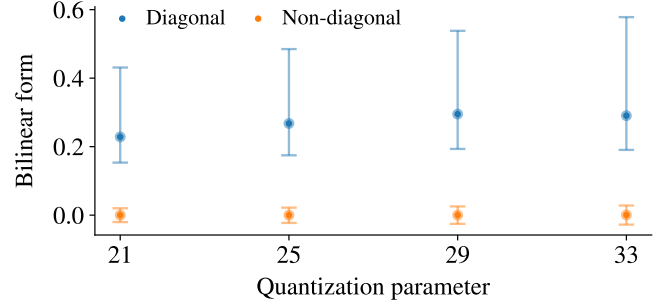


Fig. 4: Median value with 15th and 85th percentiles of the diagonal/off-diagonal terms of the bilinear forms in (12), after normalization, computed with 1000 blocks of size  $16 \times 16$  from the COCO dataset using SSE-RDO AVC.

where  $o(x)$  goes to zero at least as fast as  $x$ . At high bit-rates, we can discard the higher-order terms:

$$\|f(\hat{\mathbf{x}}(\theta)) - f(\mathbf{x})\|_2^2 \cong \|\mathbf{J}_f(\mathbf{x})(\hat{\mathbf{x}}(\theta) - \mathbf{x})\|_2^2, \quad (9)$$

where  $\cong$  denotes high bit-rate convergence [39]. As a result of this approximation, the RDO of (6) becomes

$$\theta^* = \arg \min_{\theta \in \Theta} \|\mathbf{J}_f(\mathbf{x})(\hat{\mathbf{x}}(\theta) - \mathbf{x})\|_2^2 + \lambda \sum_{i=1}^{n_b} r_i(\hat{\mathbf{x}}_i(\theta_i)). \quad (10)$$

Since this formulation requires the whole image, block-level bit allocation is still impractical. The next section addresses this problem by localizing the metric.

### C. Block-wise localization

We first write the Jacobian in terms of the sub-matrices corresponding to the pixels in each block:

$$\mathbf{J}_f(\mathbf{x}) = \begin{bmatrix} \mathbf{J}_f^{(1)}(\mathbf{x}) & \mathbf{J}_f^{(2)}(\mathbf{x}) & \dots & \mathbf{J}_f^{(n_b)}(\mathbf{x}) \end{bmatrix}, \quad (11)$$

with  $\mathbf{J}_f^{(i)}(\mathbf{x}) \in \mathbb{R}^{n_f \times n_{pb}}$ , for  $i = 1, \dots, n_b$ . Define the block-level quantization errors  $\mathbf{e}_i(\theta_i) \doteq \hat{\mathbf{x}}_i(\theta_i) - \mathbf{x}_i$ , for all  $i$ . We can write the loss as a sum of bilinear forms:

$$\|\mathbf{J}_f(\mathbf{x})(\hat{\mathbf{x}}(\theta) - \mathbf{x})\|_2^2 = \sum_{j=1}^{n_b} \sum_{i=1}^{n_b} \mathbf{e}_i(\theta_i)^\top \mathbf{J}_f^{(i)}(\mathbf{x})^\top \mathbf{J}_f^{(j)}(\mathbf{x}) \mathbf{e}_j(\theta_j). \quad (12)$$

Under the high bit-rate model [39], the expectation of cross-block terms is zero,  $\mathbb{E}_{\mathbf{e}_i, \mathbf{e}_j}(\mathbf{e}_i(\theta_i)^\top \mathbf{J}_f^{(i)}(\mathbf{x})^\top \mathbf{J}_f^{(j)}(\mathbf{x}) \mathbf{e}_j(\theta_j)) = 0$  if  $i \neq j$ . This suggests that the off-diagonal terms contribute minimally compared to the diagonal terms. As an empirical test, we compute  $\mathbf{b}_i(\mathbf{x}) = \mathbf{J}_f^{(i)}(\mathbf{x}) \mathbf{e}_i(\theta_i) / (\|\mathbf{e}_i(\theta_i)\|_2 \|\mathbf{J}_f(\mathbf{x})\|_F)$  using residuals from practical quantization levels. Then, we obtain the diagonal  $\mathbf{b}_i(\mathbf{x})^\top \mathbf{b}_i(\mathbf{x})$  and off-diagonal  $\mathbf{b}_j(\mathbf{x})^\top \mathbf{b}_i(\mathbf{x})$  bilinear forms. The diagonal terms dominate the cross-products (Fig. 4).

Thus, to convert (10) into a block-wise optimization, we approximate  $\mathbf{J}_f(\mathbf{x})^\top \mathbf{J}_f(\mathbf{x})$  by a block-diagonal matrix, which parallels diagonal curvature assumptions in the optimization

literature [40]. We call the resulting loss *input-dependent squared error* (IDSE):

$$\|\mathbf{J}_f(\mathbf{x})(\hat{\mathbf{x}}(\boldsymbol{\theta}) - \mathbf{x})\|_2^2 \approx \sum_{i=1}^{n_b} \|\mathbf{J}_f^{(i)}(\mathbf{x})(\hat{\mathbf{x}}_i(\theta_i) - \mathbf{x}_i)\|_2^2. \quad (13)$$

We can compare FD and IDSE as a function of the bit-rate in Fig. 3, where even for moderate bit-rates the linearized loss approaches FD. Now, the RDO can be formulated block-wise:

$$\theta_i^* = \arg \min_{\theta_i \in \Theta_i} \|\mathbf{J}_f^{(i)}(\mathbf{x})(\hat{\mathbf{x}}_i(\theta_i) - \mathbf{x}_i)\|_2^2 + \lambda r_i(\hat{\mathbf{x}}_i(\theta_i)), \quad (14)$$

for  $i = 1, \dots, n_b$ , which has the same form as (3). Fig. 5 compares this RDO formulation to SSE-RDO.

#### D. Randomized IDSE approximation

Computing the Jacobian is costly: we need a backward pass for each entry in  $f(\mathbf{x})$ . Since we are only interested in the distance  $\|\mathbf{J}_f(\mathbf{x})(\hat{\mathbf{x}}(\boldsymbol{\theta}) - \mathbf{x})\|_2^2$ , we propose a *randomized metric approximation method* to speed up the computation of IDSE. In particular, we compute a sketched version of the Jacobian from a lower-dimensional vector, which is obtained from the features via a metric-preserving dimensionality reduction function. We restrict our attention to linear dimensionality reduction methods  $h(\cdot)$  represented by a matrix  $\mathbf{S} \in \mathbb{R}^{n_s \times n_f}$ , such that  $h(f(\mathbf{x})) = \mathbf{S}f(\mathbf{x})$ , with  $n_s \ll n_f$ . By the chain rule, the Jacobian of the features after dimensionality reduction is:

$$\mathbf{J}_s(\mathbf{x}) \doteq \mathbf{J}_{h \circ f}(\mathbf{x}) = \mathbf{J}_h(f(\mathbf{x}))\mathbf{J}_f(\mathbf{x}) = \mathbf{S}\mathbf{J}_f(\mathbf{x}). \quad (15)$$

The matrix  $\mathbf{J}_s(\mathbf{x}) \in \mathbb{R}^{n_s \times n_p}$  is a sketch of the full Jacobian  $\mathbf{J}_f(\mathbf{x})$  with sketching matrix  $\mathbf{S}$ , which can be obtained with  $n_s$  backward passes by computing derivatives in the space of reduced dimension. In this work, we rely on the Johnson–Lindenstrauss lemma [20], [41]: given a set  $X$  of  $n_r + 1$  points, with  $n_r$  the number of RDO candidates, and provided that  $n_s \geq 8 \log(n_r)/\epsilon^2$  for some tolerance  $\epsilon > 0$ , there is a random matrix  $\mathbf{S} \in \mathbb{R}^{n_s \times n_f}$  such that, for all  $\mathbf{z}, \mathbf{y} \in X$ ,

$$(1 - \epsilon)\|\mathbf{z} - \mathbf{y}\|_2^2 \leq \|\mathbf{S}(\mathbf{z} - \mathbf{y})\|_2^2 \leq (1 + \epsilon)\|\mathbf{z} - \mathbf{y}\|_2^2, \quad (16)$$

with probability smaller than  $2 \exp(-n_s \eta(\epsilon))$ , where  $\eta(\epsilon)$  depends on the distribution of  $\mathbf{S}$  [42]; increasing  $n_s$  improves the quality of the approximation but increases the computational complexity (cf. Algorithm 1). Remarkably, the minimum number of samples needed to guarantee, with a fixed probability, that distances are preserved up to a distortion  $\epsilon$  depends on the number of RDO choices via  $n_s$  but is independent of the dimensionality of the feature space.

We choose the entries of the sketching matrix  $\mathbf{S}$  as i.i.d. Rademacher random variables [20], i.e., either +1 or -1 with equal probability. This choice balances performance [18] and memory efficiency. Since sketching the Jacobian is equivalent to sketching each of its columns in (11), we can apply block-wise localization as in (13), reaching our final IDSE-RDO formulation with the sketched Jacobian from (15):

$$\theta_i^* = \arg \min_{\theta_i \in \Theta_i} \|\mathbf{J}_s^{(i)}(\mathbf{x})(\hat{\mathbf{x}}_i(\theta_i) - \mathbf{x}_i)\|_2^2 + \lambda r_i(\hat{\mathbf{x}}_i(\theta_i)), \quad (17)$$

for  $i = 1, \dots, n_b$ . Evaluating the distortion metric in this case requires  $n_s$  inner products of the size of the block. The

formulation in (17) allows block-wise bit allocation while preserving relevant information to downstream tasks. Next, we discuss how to incorporate IDSE into a coding pipeline to balance visual quality with CV performance.

## IV. IMAGE CODING WITH IDSE

We discuss SSE regularization (Sec. IV-A), transform domain IDSE (Sec. IV-B), and Lagrangian selection (Sec. IV-C). Sec. IV-D summarizes IDSE-RDO and complexity.

### A. SSE regularization

IDSE can be combined with SSE to balance visual quality and CV performance, providing a pixel-level interpretation of the interaction between losses. Let  $\text{SSE}_{\max}$  be the maximum admissible SSE with respect to the input. We want to solve:

$$\begin{aligned} \boldsymbol{\theta}^* = \arg \min_{\boldsymbol{\theta} \in \Theta} \|\mathbf{J}_s(\mathbf{x})(\hat{\mathbf{x}}(\boldsymbol{\theta}) - \mathbf{x})\|_2^2 + \lambda \sum_{i=1}^{n_b} r_i(\hat{\mathbf{x}}_i(\theta_i)), \\ \text{such that } \|\hat{\mathbf{x}}(\boldsymbol{\theta}) - \mathbf{x}\|_2^2 \leq \text{SSE}_{\max}. \end{aligned} \quad (18)$$

Applying Lagrangian relaxation [43] and grouping together all the terms other than the rate:

$$d(\hat{\mathbf{x}}(\boldsymbol{\theta}), \mathbf{x}) = \|\mathbf{J}_s(\mathbf{x})(\hat{\mathbf{x}}(\boldsymbol{\theta}) - \mathbf{x})\|_2^2 + \tau \|\hat{\mathbf{x}}(\boldsymbol{\theta}) - \mathbf{x}\|_2^2, \quad (19)$$

where  $\tau \geq 0$  is the regularization parameter. Expanding (19),

$$d(\hat{\mathbf{x}}(\boldsymbol{\theta}), \mathbf{x}) = (\hat{\mathbf{x}}(\boldsymbol{\theta}) - \mathbf{x})^\top \mathbf{Q}_\tau(\mathbf{x})(\hat{\mathbf{x}}(\boldsymbol{\theta}) - \mathbf{x}), \quad (20)$$

with  $\mathbf{Q}_\tau(\mathbf{x}) = \mathbf{J}_s(\mathbf{x})^\top \mathbf{J}_s(\mathbf{x}) + \tau \mathbf{I}$ , for  $i = 1, \dots, n_b$ , which can be interpreted as Tikhonov regularization to the importance of each pixel—with larger  $\tau$ , we are closer to SSE.

Additionally, since the magnitude of the Jacobian changes with the feature extractor, we will need to choose different values for  $\tau$  in (19) for each  $f(\cdot)$  and  $\mathbf{x}$ , even if the relative importance of task accuracy and image representation is fixed. To simplify the selection of  $\tau$ , making it more consistent and interpretable across different  $f(\cdot)$  and  $\mathbf{x}$ , we define  $\tau = \tilde{\tau}\alpha$ , where  $\tilde{\tau}$  is a normalization factor to make the contributions of IDSE and SSE in (19) equal. As a heuristic, for the largest desirable quantization step size,  $\Delta_{\max}$ , for a given application (typically smaller than the maximum step size allowed by the codec), we choose  $\tilde{\tau}$  so that, for  $\Delta_{\max}$ ,  $\|\mathbf{J}_s(\mathbf{x})(\hat{\mathbf{x}}(\boldsymbol{\theta}) - \mathbf{x})\|_2^2 = \tilde{\tau} \|\hat{\mathbf{x}}(\boldsymbol{\theta}) - \mathbf{x}\|_2^2$ , giving both terms in (19) equal contribution to the final loss when  $\alpha = 1$  for any  $f(\cdot)$  and  $\mathbf{x}$ .

**Proposition IV.1.** For a given matrix  $\mathbf{J}_s(\mathbf{x})$ ,

$$\tilde{\tau} = \|\mathbf{J}_s(\mathbf{x})\|_2^2, \quad (21)$$

ensures  $\max_{\boldsymbol{\theta}} \|\mathbf{J}_s(\mathbf{x})(\hat{\mathbf{x}}(\boldsymbol{\theta}) - \mathbf{x})\|_2^2 = \tilde{\tau} \max_{\boldsymbol{\theta}} \|\hat{\mathbf{x}}(\boldsymbol{\theta}) - \mathbf{x}\|_2^2$ .

*Proof.* The regularizer is given by the ratio:

$$\tilde{\tau} = \max_{\boldsymbol{\theta}} \|\mathbf{J}_s(\mathbf{x})(\hat{\mathbf{x}}(\boldsymbol{\theta}) - \mathbf{x})\|_2^2 / \max_{\boldsymbol{\theta}} \|\hat{\mathbf{x}}(\boldsymbol{\theta}) - \mathbf{x}\|_2^2. \quad (22)$$

By definition of spectral norm, and assuming the set of coding options is dense, there is an error that reaches the upper bound:

$$\|\mathbf{J}_s(\mathbf{x})(\hat{\mathbf{x}}(\boldsymbol{\theta}) - \mathbf{x})\|_2^2 \leq \|\mathbf{J}_s(\mathbf{x})\|_2^2 \|\hat{\mathbf{x}}(\boldsymbol{\theta}) - \mathbf{x}\|_2^2. \quad (23)$$

The result follows since  $\mathbf{J}_s(\mathbf{x})$  does not depend on  $\boldsymbol{\theta}$ .  $\square$

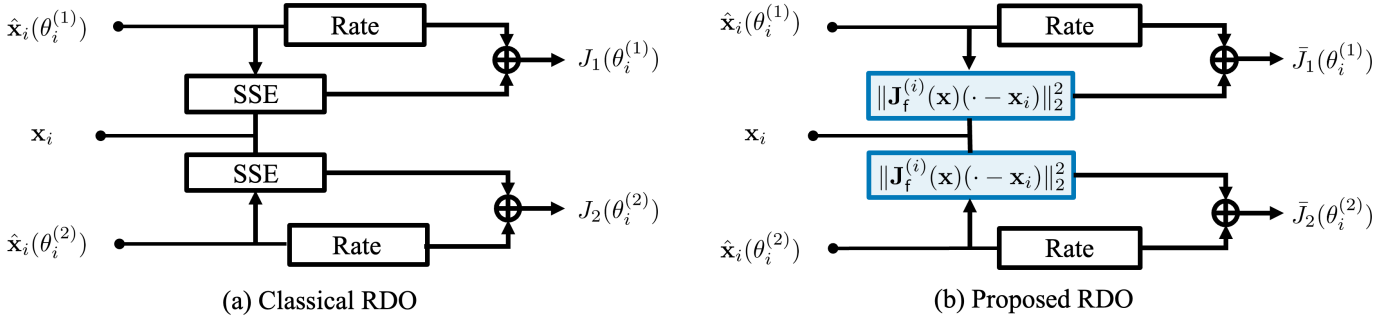


Fig. 5: Process of comparing two RDO options,  $\theta_i^{(1)}$  and  $\theta_i^{(2)}$ , using (a) classical SSE-RDO and (b) our proposed IDSE-RDO.

This choice of  $\tau$  can adapt to the characteristics of the content and the feature extractor. In our setup, we set  $\tau = \alpha \tilde{\tau}$ , testing different values of  $\alpha$  in our experiments to explore different trade-offs between visual quality and downstream task performance (cf. Table IV).

### B. Transform domain evaluation

Let  $\mathbf{U}$  be an orthogonal transform, such as the discrete cosine transform (DCT) or the asymmetric discrete sine transform (ADST) [44]. Define  $\mathbf{y}_i \doteq \mathbf{U}^\top \mathbf{x}_i$ , with  $\hat{\mathbf{y}}_i(\theta_i)$  its quantized version. Then, IDSE becomes:

$$d(\hat{\mathbf{y}}_i(\theta_i), \mathbf{y}_i) = \|\mathbf{B}^{(i)}(\mathbf{x})(\hat{\mathbf{y}}_i(\theta_i) - \mathbf{y}_i)\|_2^2, \quad (24)$$

where  $\mathbf{B}^{(i)}(\mathbf{x}) \doteq \mathbf{J}_s^{(i)}(\mathbf{x})\mathbf{U}$ , for  $i = 1, \dots, n_b$ , is the transform-domain version of the sketched Jacobian. Thus, RDO can be conducted directly in the transform domain:

$$\theta_i^* = \arg \min_{\theta_i \in \Theta_i} d(\hat{\mathbf{y}}_i(\theta_i), \mathbf{y}_i) + \lambda r_i(\hat{\mathbf{y}}_i(\theta_i)). \quad (25)$$

Therefore, the RD cost can be evaluated using (25), which is more efficient than using (17). Since, by Parseval's identity, SSE can be computed in transform domain, the same property extends to the regularized version of IDSE in (20).

### C. Lagrange multiplier

The Lagrangian in (4) is based on a simplified logarithmic model relating the expected rate to the expected SSE. Since we are replacing the latter with a different metric, this relationship no longer holds. We can derive an expression for  $\lambda$  based on the expected value of the regularized IDSE in a given block: at high-rates [39], using quantization step  $\Delta$ ,

$$D_i = \mathbb{E}_{\hat{\mathbf{x}}, \mathbf{x}}(d(\hat{\mathbf{x}}_i, \mathbf{x}_i)) = (\mathbb{E}_{\mathbf{x}}(\|\mathbf{J}_s^{(i)}(\mathbf{x})\|_F^2) + n\tau) \frac{\Delta^2}{12}, \quad (26)$$

for  $i = 1, \dots, n_b$ . Assuming the block Jacobians in the image are i.i.d., we obtain  $D = D_i$ . The logarithmic model in [16] states that  $R(D) = a n \log(bn/D)$ , where  $a$  and  $b$  are related to the entropy power of the source. Then,  $\lambda = D/(na)$ , and using the relationship between QP,  $\Delta$ , and  $\lambda$  in AVC [45],

$$\lambda = c \left( \sum_{i=1}^{n_b} \|\mathbf{J}_s^{(i)}(\mathbf{x})\|_F^2 / (nn_b) + \tau \right) 2^{(\text{QP}-12)/3}. \quad (27)$$

Experimentally, setting  $c$  as in (4) led to good rate control.

### Algorithm 1 Jacobian sketching

- 1: **Input:** Feature extractor  $f(\cdot)$ , num. samples  $n_s$ , image  $\mathbf{x}$
- 2: Evaluate  $f(\mathbf{x}) \in \mathbb{R}^{n_f}$   $\triangleright$  Compute features
- 3: **for**  $i = 1$  to  $n_s$  **do**
- 4:  $\mathbf{s}_i \sim \text{Rademacher}(n_f)$   $\triangleright$   $n_f$ -vector, fair coin flips
- 5:  $q_i(\mathbf{x}) \leftarrow \mathbf{s}_i^\top f(\mathbf{x})$
- 6: Get  $\nabla_{\mathbf{x}} q_i(\mathbf{x})$  via autodiff
- 7: **end for**
- 8:  $\mathbf{J}_s(\mathbf{x}) \leftarrow [\nabla_{\mathbf{x}} q_1(\mathbf{x}) \quad \dots \quad \nabla_{\mathbf{x}} q_{n_s}(\mathbf{x})]^\top$
- 9: **return**  $\mathbf{J}_s(\mathbf{x})$

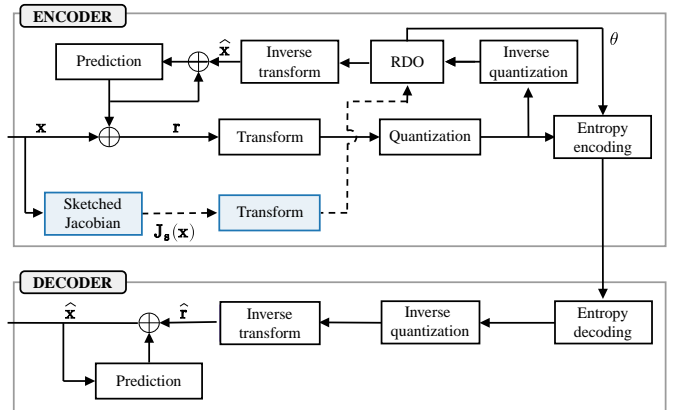


Fig. 6: Block diagram of the proposed codec, with the steps needed for IDSE-RDO in blue. Since we do not modify the decoder, it remains compatible with standardized codecs.

### D. RDO with IDSE

In our proposed codec (Fig. 6), given an input  $\mathbf{x}$ , we compute  $f(\mathbf{x})$ , obtain the sketched Jacobian  $\mathbf{J}_s(\mathbf{x})$  (Algorithm 1), divide it into blocks  $\mathbf{J}_s^{(i)}(\mathbf{x})$ , for  $i = 1, \dots, n_b$ , and compute its transform. Next, we encode each block of the input using different coding tools (Fig. 5) and perform RDO using (25) or its regularized version.

We compare now the complexity of our proposed method and block FD in terms of floating point operations (FLOPs), with runtimes given in Sec. V-C. We first compute the sketched Jacobian, which requires a forward pass and  $n_s$  backward passes—a backward pass having roughly twice the cost of a forward pass [46]. To evaluate the network, we resize the

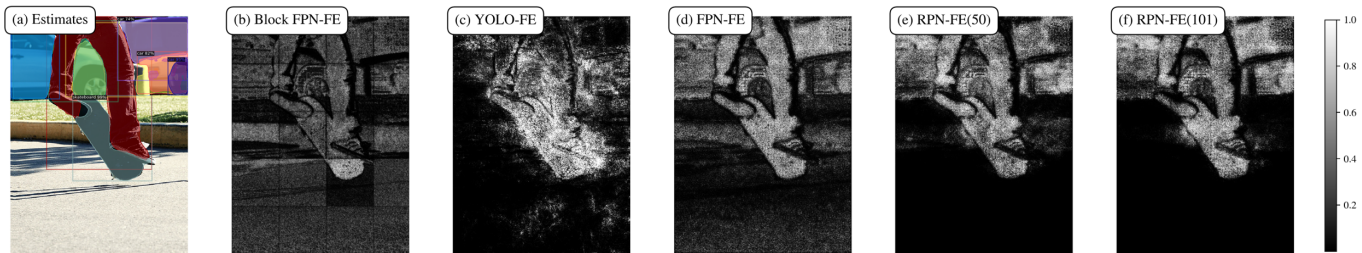


Fig. 7: (a) Mask R-CNN estimates; (b-f)  $\text{diag}(\mathbf{J}_s(\mathbf{x})^T \mathbf{J}_s(\mathbf{x}))$ , reshaped and scaled, obtained by (b) localizing block-wise first and then expanding the metric, using blocks of size  $128 \times 128$  and a FPN-FE; (c-f) using our approach with different feature extractors. Lighter regions are more important; using the whole image and deeper models emphasizes relevant regions.

images to the size used during training. During encoding, we need to evaluate IDSE, with complexity  $n_s$  times larger than the complexity of SSE. To compute block FD [17], we have to evaluate the DNN and compute the distance in feature space—which may be higher-dimensional than pixel space—for each RDO candidate. In this case, no resizing is applied.

Assume the input has  $h \times w$  pixels, and after resizing to compute the Jacobian, we get images of  $h' \times w'$  pixels; also, let  $n_r$  be the number of RDO candidates. Let  $C$  be the cost of the forward pass in terms of floating point operations per pixel (FLOPs/px). We use the same feature extractor for both approaches. Using block FD, we require  $h \times w \times (n_r + 1) \times C$  FLOPs to evaluate the cost throughout the image. We require  $h' \times w' \times (2n_s + 1) \times C$  FLOPs to sample the Jacobian. Assuming image sizes of  $768 \times 768$  pixels, resized images of size  $224 \times 224$ ,  $n_r = 18$  (9 quantization steps and 2 block partitions), and letting  $n_s = 4$ , our method reduces the number of FLOPs with respect to block FD by a factor of 24.81.

Regarding memory, the encoder for IDSE-RDO has complexity  $O(n_s n_p)$  since it stores  $n_s$  vectors of the size of the image. Although the values of  $n_s$  we consider make the memory overhead manageable, future work may explore options to further improve memory complexity (Sec. VI).

## V. EMPIRICAL EVALUATION

We test object detection/instance segmentation in the COCO 2017 validation set [21] and the PennFudan dataset [22]. Since the tasks use images in 4:4:4 format, we use AVC baseline in 4:4:4 format to ensure convergence to the performance of the uncompressed image. We apply IDSE-RDO to the luminance channel; for the chroma channels, we use SSE-RDO, setting a QP offset of +3. We use an Intel(R) E5-2667 v4 with an NVIDIA GeForce RTX 3090 (24GB VRAM). The RDO decides block-partitioning ( $4 \times 4$  or  $16 \times 16$ ) and quantization step ( $\Delta\text{QP} = -4, -3, \dots, 3, 4$ ), i.e., the effective quantization step is derived from  $\text{QP} + \Delta\text{QP}$ . We report 1) mean average precision (mAP@[0.5:0.05:0.95]), 2) Y-PSNR, and 3) Y-MS-SSIM [47]. We set  $n_s = 8$  in (15). By default, the downstream DNN is a Mask R-CNN with ResNet-50 [48], and we set  $\tau = \tilde{\tau}$  from (21).

We evaluate four different feature extractors. Three of them are based on Mask R-CNN [48]: the coarsest output (P6) of an FPN [31], which we call FPN-FE, and the outputs of the RPN, which we call RPN-FE. For RPN-FE, we will consider a

Mask R-CNN with ResNet-50 (RPN-FE(50)) and a Mask R-CNN with ResNet-101 (RPN-FE(101)) [49]. The last feature extractor is the backbone of YOLOv9 [50] (YOLO-FE).

We explore the effect of the feature extractor and regularization (Sec. V-A), as well as the coding performance in different tasks (Sec. V-B). Finally, we discuss complexity (Sec. V-C).

### A. Feature extractor and regularization

We consider 1000 images from COCO [21] and compress them with quality parameter  $\text{QP} \in \{27, 30, 33, 36, 39\}$ .

1) *Importance maps*: To assess the effect of using different feature extractors, we depict pixel importance maps in Fig. 7. The feature extractors for RPN-FE(50) and RPN-FE(101) are deeper and discriminate better the regions in the image that are important for the target task. Our method applies Taylor’s expansion first and then localizes the metric. An alternative is to localize the metric block-wise first, as in block FD [17], and then apply Taylor’s expansion to each block as in Sec. III-B. However, as Fig. 7 (b) shows, evaluating the feature extractor block-wise leads to estimates of the importance that do not match exactly the position of the objects. We also depict the  $\Delta\text{QP}$  chosen block-wise for compressing an image with  $\text{QP} = 29$  using SSE-RDO and IDSE-RDO with RPN-FE(50) (Fig. 8). IDSE-RDO allocates more bit-rate to relevant regions for the downstream task.

2) *Different models*: We consider three downstream DNNs: Mask R-CNN with ResNet-50 and ResNet-101 [49], and YOLOv9 [50], which is more efficient and might be better suited for low-cost edge devices [7] (cf. Sec. V-C). For IDSE-RDO, we use RPN-FE(50), RPN-FE(101), and YOLO-FE, which correspond to the early stages of the three downstream DNNs we use, and then evaluate each of these systems using the compressed images. We show the BD rate savings [51] with respect to SSE-RDO [51] for each possible configuration in Table III. We conclude that IDSE-RDO provides coding gains for all the downstream DNNs we consider, regardless of the feature extractor.

3) *Regularization*: To explore the trade-off between visual quality and CV performance, we test our method with different values of  $\tau = \alpha\tilde{\tau}$ . We summarize our results with IDSE-RDO using RPN-FE(50) in Table IV. Our setup provides fine-grained control of the trade-off between visual quality and downstream task performance. By sacrificing the former, we can reach bit-rate savings of up to 10% in the latter.

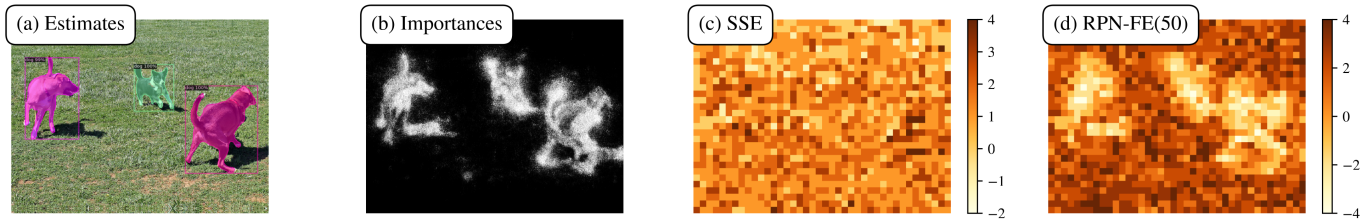


Fig. 8: (a) Mask R-CNN estimates; (b) importances for RPN-FE(50); (c-d)  $\Delta QP$  chosen by RDO with (c) SSE and (d) IDSE-RPN-FE(50). Lower  $\Delta QP$  implies finer quantization. IDSE-RDO preserves relevant regions for the downstream task.

	Visual quality		Mask R-CNN				YOLOv9	
	PSNR $\downarrow$	MS-SSIM $\downarrow$	ResNet-50		ResNet-101		mAP det. $\downarrow$	mAP seg. $\downarrow$
			mAP det. $\downarrow$	mAP seg. $\downarrow$	mAP det. $\downarrow$	mAP seg. $\downarrow$		
RPN-FE(50)	2.05	2.32	-8.65	-9.30	-8.26	-8.60	-7.47	-6.45
RPN-FE(101)	<b>1.92</b>	2.44	<b>-9.63</b>	<b>-9.65</b>	<b>-8.45</b>	<b>-9.14</b>	<b>-7.50</b>	<b>-6.55</b>
YOLO-FE	2.53	<b>1.96</b>	-6.92	-7.38	-5.85	-6.16	-5.34	-6.00

Table III: BD-rate savings [%] with respect to SSE-RDO using IDSE-RDO. Lower is better  $\downarrow$ . We compute mAP for object detection (mAP det.) and instance segmentation (mAP seg.) using Mask R-CNN with ResNet-50 and ResNet-101, as well as YOLOv9. The best results for each column appear in **blue**. IDSE-RDO outperforms SSE-RDO for any configuration.

Regularization	PSNR $\downarrow$	MS-SSIM $\downarrow$	Det. $\downarrow$	Seg. $\downarrow$
$\tau = 3\tilde{\tau}/2$	<b>0.86</b>	<b>2.40</b>	-7.82	-8.24
$\tau = \tilde{\tau}$	2.05	2.32	-8.65	-9.30
$\tau = 2\tilde{\tau}/3$	2.53	4.09	<b>-9.93</b>	<b>-10.01</b>

Table IV: BD-rate savings [%] with respect to SSE-RDO. Lower is better  $\downarrow$ . For IDSE-RDO, we use RPN-FE(50) with different  $\tau$ . The best values for each column appear in **blue**. Larger  $\tau$  improves PSNR but reduces mAP performance.

## B. Assessing different tasks

1) *COCO and transfer learning*: We use IDSE-RDO with FPN-FE and RPN-FE(50). We also consider RDO with block FD in a setup inspired by [17], using as a distortion metric the average of the block FD in the 5th layer of VGG and the SSE. However, [17] used block sizes of  $128 \times 128$  pixels while, due to codec and resolution constraints, we use blocks of size  $16 \times 16$  pixels. To assess this approximation, we evaluate the feature distance using blocks of  $128 \times 128$  pixels (the original metric [17]) and the aggregate of the 64 sub-blocks of  $16 \times 16$  pixels (our approximation). Correlation results (Fig. 9) suggest the approximation is reasonable. As proposed in [17], we implement block FD using the sum of absolute differences between the features rather than the square difference, and we set  $c = 0.57$  in (4), which also yields the best results in our setup. As in [17], we re-scale the Lagrangian based on the ratio between SSE and block FD for the first block.

Beyond images from COCO, we also follow a transfer learning approach, where we use the FPN from Mask R-CNN as a first step, and then we fine-tune the last layers to detect and segment pedestrians. For fine-tuning, we freeze the feature extractor and train the region proposal layers for 5 epochs using a training set of 50 images. We use the remaining 50 images for testing. In this case, we compress with  $QP \in \{31, 33, 35, 37, 39\}$  because task performance

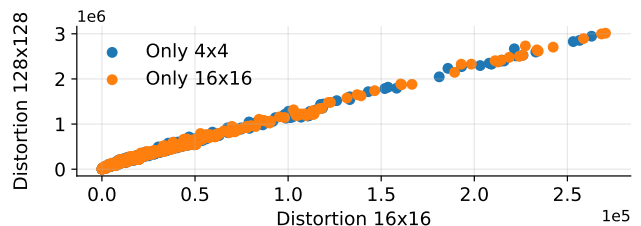


Fig. 9: Block FD with blocks of  $128 \times 128$  pixels (original [17]) and the corresponding 64 sub-blocks of  $16 \times 16$  (approximation). To remove the effect of RDO, we use only  $4 \times 4$  or  $16 \times 16$  block partitions. The Pearson correlation coefficient is 0.997 for both setups.

	Method	PSNR $\downarrow$	MS-SSIM $\downarrow$	Det. $\downarrow$	Seg. $\downarrow$
COCO	FPN-FE	<b>1.32</b>	<b>-3.36</b>	-6.06	-5.93
	RPN-FE(50)	2.05	2.32	<b>-8.65</b>	<b>-9.30</b>
	Block FD	1.84	-0.91	-2.18	-2.23
PF	FPN-FE	<b>0.42</b>	<b>-4.74</b>	-7.31	-6.00
	RPN-FE(50)	0.64	0.94	<b>-9.50</b>	<b>-6.87</b>
	Block FD	0.68	-1.26	-4.25	-3.21

Table V: BD-rate savings [%] with respect to SSE-RDO. Lower is better  $\downarrow$ . The best method for each metric appears in **blue**. Our methods outperform SSE-RDO and block FD-RDO. RPN-FE(50) performs the best in CV tasks.

saturates for smaller QP. RD curves (Fig. 10) and BD-rates (Table V) for COCO and PennFudan show that, for a similar performance in PSNR, IDSE-RDO yields coding gains with respect to block FD for mAP. Using RPN-FE(50) provides better mAP performance than FPN-FE since the former incorporates more information about the target task.

2) *Mismatched models and self-supervised learning*: When the feature extractor does not match the downstream DNN, we expect our system to underperform. In this scenario, in



$f(\cdot)$	PSNR ↓	MS-SSIM ↓	People		Fruits	
			Det. ↓	Seg. ↓	Det. ↓	Seg. ↓
SSL	<b>0.85</b>	<b>-3.67</b>	<b>-3.01</b>	<b>-3.08</b>	<b>-4.27</b>	<b>-4.11</b>
SL-People	1.04	<b>-2.90</b>	<b>-5.33</b>	<b>-4.62</b>	-3.01	-3.04
SL-Fruits	<b>0.91</b>	-2.44	-2.20	-1.94	<b>-6.61</b>	<b>-4.32</b>

Table VI: BD-rate savings [%] with respect to SSE-RDO for people detection/segmentation and fruit detection/segmentation. SL stands for supervised learning. Lower is better ↓. The best method for each metric appears in **blue**, the second best in **orange**.

which our information about the task is limited, we can rely on a feature extractor trained by SSL using augmentations that encode generic properties, such as rotational invariance. To test this idea, we construct two datasets from the COCO2017 validation set: a people dataset and a fruit dataset, each comprising 200 images. We fine-tune a Mask R-CNN with a ResNet-50 to each dataset using subsets of 100 images. We use these two systems as our downstream DNNs.

We compress images with three FPN-FE: the FPNs from the two fine-tuned Mask R-CNNs above, and an additional FPN trained via SSL [12] using geometric augmentations, which should be suitable for both person/fruit detection. We show the performance for each FPN-FE in Table VI for the remaining 100 images of each dataset. The fine-tuned FPN-FEs reach the best results for the tasks they were trained for, while the SSL-based FPN-FE is the second best in both cases. If the feature extractor does not match the downstream DNN, we still have coding gains, but the performance drops.

### C. Computational complexity

We show the runtime to compute the Jacobian in Table VII. We obtain our results as the average for 100 images of the COCO dataset [21] for YOLO-FE, RPN-FE (50), and RPN-FE (101). For all feature extractors, the computational complexity scales linearly with the number of samples used to sketch the Jacobian. We also compute the runtime overhead of considering IDSE-RDO over SSE-RDO. We compute the runtime of both computing the Jacobian and encoding the image using IDSE-RDO, and we measure the increase with respect to the runtime of using SSE-RDO. The worst case overhead is 11.02%. Using block FD for RDO as discussed in Sec. V-B, the computational overhead in the encoder is 89%.

## VI. CONCLUSION

In this paper, we proposed an RDO method that preserves the feature distance (FD). Using linearization arguments and a localization assumption, we simplified the FD to an input-dependent squared error loss involving the Jacobian of the feature extractor. To further reduce complexity, we considered a sketching strategy for the Jacobian. The resulting loss can be computed block-wise and in the transform domain. The Jacobian can be obtained before compressing the image, which provides computational advantages. We validated our method using AVC, showing coding gains for computer vision tasks with a small computational overhead.

	$f(\cdot)$	$n_s = 2$	$n_s = 4$	$n_s = 8$	$n_s = 16$
		<b>Compute Jacobian</b>	RPN-FE (50)	<b>0.097</b>	<b>0.162</b>
	RPN-FE (101)	0.123	0.206	0.368	0.699
	YOLO-FE	<b>0.063</b>	<b>0.097</b>	<b>0.168</b>	<b>0.307</b>
<b>Encoder overhead</b>	RPN-FE (50)	<b>2.67%</b>	<b>4.13%</b>	<b>7.24%</b>	<b>11.55%</b>
	RPN-FE (101)	3.22%	4.94%	7.39%	12.02%
	YOLO-FE	<b>2.04%</b>	<b>3.72%</b>	<b>7.15%</b>	<b>10.27%</b>

Table VII: Average runtime [s] to compute  $\mathbf{J}_s(\mathbf{x})$  for different  $n_s$  (top) and increase in encoder runtime [%] with respect to SSE-RDO (bottom). In both cases, lower is better. The best values for each column appear in **blue**, the second best in **orange**. YOLO-FE is the most efficient, followed by RPN-FE (50) and RPN-FE (101).

Future work will focus on memory consumption. For instance, using the importance maps has memory complexity  $O(n_p)$ . To improve upon this result, we can apply vector quantization to the importance maps [52] or use quantized versions of the Johnson-Lindenstrauss lemma [42]. Other extensions include IDSE for feature compression [6], transform design [44], and quality saturation detection [53], as well as extending our work to recent codecs such as VVC [23]. Although we expect the results to be similar, codecs with multiple transforms may further increase the memory overhead.

## REFERENCES

- [1] H. Choi and I. V. Bajić, “Scalable image coding for humans and machines,” *IEEE Trans. Image Process.*, vol. 31, pp. 2739–2754, 2022.
- [2] Y. Zhang, C. Rosewarne, S. Liu, and C. Hollmann, “Call for evidence for video coding for machines,” *ISO/IEC JTC 1/SC 29/WG. 2*, 2022.
- [3] J. Ascenso, E. Alshina, and T. Ebrahimi, “The JPEG AI standard: Providing efficient human and machine visual data consumption,” *IEEE MultiMedia*, vol. 30, no. 1, pp. 100–111, 2023.
- [4] A. Ortega, B. Beferull-Lozano, N. Srinivasamurthy, and H. Xie, “Compression for recognition and content-based retrieval,” in *Proc. Europ. Sig. Process. Conf.*, 2000, pp. 1–4.
- [5] Y. LeCun, Y. Bengio, and G. Hinton, “Deep learning,” *Nature*, vol. 521, no. 7553, pp. 436–444, 2015.
- [6] H. Choi and I. V. Bajić, “Deep feature compression for collaborative object detection,” in *Proc. IEEE Int. Conf. Image Process.* 2018, pp. 3743–3747, IEEE.
- [7] H. Choi and I. V. Bajić, “High efficiency compression for object detection,” in *Proc. IEEE Int. Conf. Acoust., Speech, and Signal Process.* 2018, pp. 1792–1796, IEEE.
- [8] N. Le, H. Zhang, F. Cricri, R. Ghaznavi-Youvalari, et al., “Learned image coding for machines: A content-adaptive approach,” in *Proc. IEEE Int. Conf. Mult. and Expo.* July 2021, pp. 1–6, IEEE.
- [9] N. Tishby, F. C. Pereira, and W. Bialek, “The information bottleneck method,” in *Proc. Annu. Allerton Conf. Commun., Control, and Comput., Urbana-Champaign, IL*, 1999, pp. 368–377.
- [10] Y. Dubois, B. Bloem-Reddy, K. Ullrich, and C. J. Maddison, “Lossy compression for lossless prediction,” *Proc. Adv. Neural Inf. Process. Sys.*, vol. 34, pp. 14014–14028, 2021.
- [11] M. A. F. Hossain, Z. Duan, Y. Huang, and F. Zhu, “Flexible variable-rate image feature compression for edge-cloud systems,” in *Proc. Intl. Conf. on Mult. and Expo Works.* IEEE, 2023, pp. 182–187.
- [12] A. Bardes, J. Ponce, and Y. LeCun, “Vicreg: Variance-invariance-covariance regularization for self-supervised learning,” in *Proc. Intl. Conf. on Learn. Repres.*, 2021.
- [13] Z. Duan and F. M. Zhu, “Compression of self-supervised representations for machine vision,” in *Proc. IEEE Intl. Works. on Mult. Sign. Process.*, 2024, pp. 1–6.
- [14] W. Jiang, H. Choi, and F. Racapé, “Adaptive human-centric video compression for humans and machines,” in *Proc. IEEE/CVF Conf. Comput. Vis. Pattern Recog.*, 2023, pp. 1121–1129.

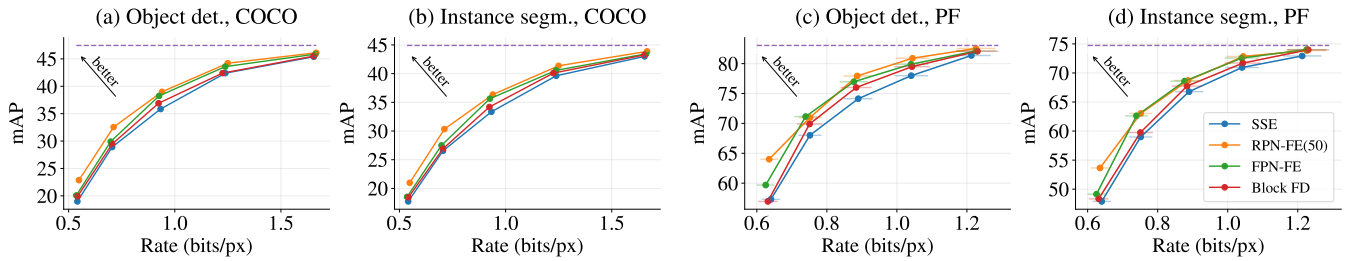


Fig. 10: Rate-distortion curves for object detection and instance segmentation mAP using SSE-RDO, our proposed IDSE-RDO with FPN-FE and RPN-FE (50), and RDO using block FD on images from the COCO dataset (a–b) and the PennFudan dataset (c–d). We added the standard error on the estimation of the average bit-rate as a horizontal bar.

- [15] A. Ortega and K. Ramchandran, “Rate-distortion methods for image and video compression,” *IEEE Signal Process. Mag.*, vol. 15, no. 6, pp. 23–50, Nov. 1998.
- [16] G. J. Sullivan and T. Wiegand, “Rate-distortion optimization for video compression,” *IEEE Signal Process. Mag.*, vol. 15, no. 6, pp. 74–90, 1998.
- [17] K. Fischer, F. Brand, C. Herglotz, and A. Kaup, “Video coding for machines with feature-based rate-distortion optimization,” in *Proc. IEEE Int. Work. Mult. Signal Process.* Sept. 2020, pp. 1–6, IEEE.
- [18] S. Fernández-Menduiña, E. Pavez, and A. Ortega, “Feature-preserving rate-distortion optimization in image coding for machines,” in *Proc. IEEE Intl. Work. on Mult. Sign. Process.*, 2024, pp. 1–6.
- [19] S. Jain, H. Salman, A. Khaddaj, E. Wong, et al., “A data-based perspective on transfer learning,” in *Proc. IEEE/CVF Conf. Comput. Vis. Pattern Recog.*, 2023, pp. 3613–3622.
- [20] D. Achlioptas, “Database-friendly random projections: Johnson-Lindenstrauss with binary coins,” *Journal of Comput. and Sys. Sciences*, vol. 66, no. 4, pp. 671–687, 2003.
- [21] T.-Y. Lin, M. Maire, S. Belongie, J. Hays, et al., “Microsoft coco: Common objects in context,” in *Proc. European Conf. Comp. Vis.* Springer, 2014, pp. 740–755.
- [22] L. Wang, J. Shi, G. Song, and I.-f. Shen, “Object detection combining recognition and segmentation,” in *Proc. Asian Conf. on Comput. Vis.* Springer, 2007, pp. 189–199.
- [23] B. Bross, Y.-K. Wang, Y. Ye, S. Liu, et al., “Overview of the versatile video coding (VVC) standard and its applications,” *IEEE Trans. on Circ. and Sys. for Video Techn.*, vol. 31, no. 10, pp. 3736–3764, 2021.
- [24] J. Ballé, P. A. Chou, D. Minnen, S. Singh, et al., “Nonlinear transform coding,” *IEEE Journal of Sel. Top. in Sig. Process.*, vol. 15, no. 2, pp. 339–353, 2020.
- [25] T. Ladune, P. Philippe, F. Henry, G. Clare, and T. Leguay, “Cool-chic: Coordinate-based low complexity hierarchical image codec,” in *Proc. IEEE/CVF Conf. Comput. Vis. Pattern Recog.*, 2023, pp. 13515–13522.
- [26] H. Li and X. Zhang, “Human-machine collaborative image compression method based on implicit neural representations,” *IEEE Journal on Emerg. and Select. Tops. in Circs. and Sys.*, 2024.
- [27] J. Ballé, L. Versari, E. Dupont, H. Kim, and M. Bauer, “Good, cheap, and fast: Overfitted image compression with Wasserstein distortion,” *arXiv preprint arXiv:2412.00505*, 2024.
- [28] N. Le, H. Zhang, F. Cricri, R. Ghaznavi-Youvalari, and E. Rahtu, “Image coding for machines: an end-to-end learned approach,” in *Proc. IEEE Int. Conf. Acoust., Speech, and Signal Process.* June 2021, pp. 1590–1594, IEEE.
- [29] J. I. Ahonen, R. G. Youvalari, N. Le, H. Zhang, et al., “Learned enhancement filters for image coding for machines,” in *Proc. IEEE Intl. Symp. on Mult. IEEE*, 2021, pp. 235–239.
- [30] X. Luo, H. Talebi, F. Yang, M. Elad, and P. Milanfar, “The rate-distortion-accuracy tradeoff: JPEG case study,” *arXiv preprint arXiv:2008.00605*, 2020.
- [31] T.-Y. Lin, P. Dollár, R. Girshick, K. He, et al., “Feature pyramid networks for object detection,” in *Proc. IEEE/CVF Conf. Comput. Vis. Pattern Recog.*, 2017, pp. 2117–2125.
- [32] A. Gou, H. Sun, X. Zeng, and Y. Fan, “Fast VVC intra encoding for video coding for machines,” in *Proc. IEEE Int. Symp. Circ. and Sys.* May 2023, pp. 1–5, IEEE.
- [33] A. Paszke, S. Gross, S. Chintala, G. Chanan, et al., “Automatic differentiation in Pytorch,” 2017.
- [34] D. J. Ringis, Vibhoothi, F. Pitié, and A. Kokaram, “The disparity between optimal and practical Lagrangian multiplier estimation in video encoders,” *Front. in Signal Process.*, vol. 3, pp. 1205104, 2023.
- [35] A. Tarvainen and H. Valpola, “Mean teachers are better role models: Weight-averaged consistency targets improve semi-supervised deep learning results,” in *Proc. Adv. Neural Inf. Process. Sys.*, 2017, vol. 30.
- [36] L. Béthune, T. Boissin, M. Serrurier, F. Mamalet, et al., “Pay attention to your loss: understanding misconceptions about Lipschitz neural networks,” in *Proc. Adv. Neural Inf. Process. Sys.*, 2022, vol. 35, pp. 20077–20091.
- [37] A. Virmaux and K. Scaman, “Lipschitz regularity of deep neural networks: analysis and efficient estimation,” in *Proc. Adv. Neural Inf. Process. Sys.*, 2018, vol. 31.
- [38] A. Jacot, F. Gabriel, and C. Hongler, “Neural tangent kernel: Convergence and generalization in neural networks,” *Proc. Adv. Neural Inf. Process. Sys.*, vol. 31, 2018.
- [39] H. Gish and J. Pierce, “Asymptotically efficient quantizing,” *IEEE Trans. Inform. Theory*, vol. 14, no. 5, pp. 676–683, 1968.
- [40] J. Martens and R. Grosse, “Optimizing neural networks with Kronecker-factored approximate curvature,” in *Proc. Intl. Conf. on Mach. Learn.* PMLR, 2015, pp. 2408–2417.
- [41] W. B. Johnson, J. Lindenstrauss, et al., “Extensions of Lipschitz mappings into a Hilbert space,” *Contemporary mathematics*, vol. 26, no. 189–206, pp. 1, 1984.
- [42] L. Jacques, “A quantized Johnson–Lindenstrauss lemma: The finding of Buffon’s needle,” *IEEE Transactions on Information Theory*, vol. 61, no. 9, pp. 5012–5027, 2015.
- [43] H. Everett III, “Generalized Lagrange multiplier method for solving problems of optimum allocation of resources,” *Operations research*, vol. 11, no. 3, pp. 399–417, 1963.
- [44] S. Fernández-Menduiña, E. Pavez, and A. Ortega, “Fast DCT+: A family of fast transforms based on rank-one updates of the path graph,” in *Proc. IEEE Int. Conf. Acoust., Speech, and Signal Process.*, 2025.
- [45] T. Wiegand, G. Sullivan, G. Bjontegaard, and A. Luthra, “Overview of the H.264/AVC video coding standard,” *IEEE Trans. Circuits Syst. Video Technol.*, vol. 13, no. 7, pp. 560–576, July 2003.
- [46] Y. Sepelri, P. Pad, A. C. Yüzügüler, P. Frossard, and L. A. Dunbar, “Hierarchical training of deep neural networks using early exiting,” *IEEE Trans. on Neural Nets. and Learn. Sys.*, pp. 1–15, 2024.
- [47] Z. Wang, E. P. Simoncelli, and A. C. Bovik, “Multiscale structural similarity for image quality assessment,” in *Proc. Asilomar Conf. on Signals, Sys. & Comput.* IEEE, 2003, vol. 2, pp. 1398–1402.
- [48] K. He, G. Gkioxari, P. Dollár, and R. Girshick, “Mask R-CNN,” in *Proc. IEEE/CVF Conf. Comput. Vis. Pattern Recog.*, 2017, pp. 2961–2969.
- [49] S. Xie, R. Girshick, P. Dollár, Z. Tu, and K. He, “Aggregated residual transformations for deep neural networks,” in *Proc. IEEE/CVF Conf. Comput. Vis. Pattern Recog.*, 2017, pp. 1492–1500.
- [50] C.-Y. Wang, I.-H. Yeh, and H.-Y. Mark Liao, “Yolov9: Learning what you want to learn using programmable gradient information,” in *Euro. conf. on comp. vis.* Springer, 2024, pp. 1–21.
- [51] G. Bjontegaard, “Calculation of average PSNR differences between RD-curves,” *ITU SG16 Doc. VCEG-M33*, 2001.
- [52] S. Fernández-Menduiña, E. Pavez, and A. Ortega, “Image coding via perceptually inspired graph learning,” in *Proc. IEEE Int. Conf. Image Process.* IEEE, 2023, pp. 2495–2499.
- [53] X. Xiong, E. Pavez, A. Ortega, and B. Adsumilli, “Rate-distortion optimization with alternative references for UGC compression,” in *Proc. IEEE Int. Conf. Acoust., Speech, and Signal Process.*, 2023, pp. 1–5.